Copper Metallization of Gold Nanostructure Activated Polypyrrole by Electroless Deposition

Pandey, Richa; Jian, Nan; Inberg, Alexandra; Palmer, Richard; Shacham-Diamand, Yosi

DOI:
10.1016/j.electacta.2017.06.157

Document Version
Peer reviewed version

Citation for published version (Harvard):
Pandey, R, Jian, N, Inberg, A, Palmer, R & Shacham-Diamand, Y 2017, 'Copper Metallization of Gold Nanostructure Activated Polypyrrole by Electroless Deposition', *Electrochimica Acta*, vol. 246, pp. 1210-1216. https://doi.org/10.1016/j.electacta.2017.06.157

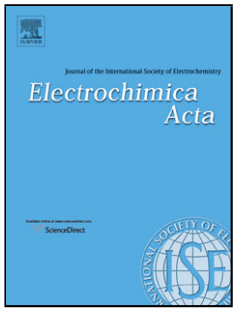

Title: Copper Metallization of Gold Nanostructure Activated Polypyrrole by Electroless Deposition

Authors: Richa Pandey, Nan Jian, Alexandra Inberg, Richard E. Palmer, Yosi Shacham-Diamand

PII: S0013-4686(17)31395-6
DOI: http://dx.doi.org/doi:10.1016/j.electacta.2017.06.157
Reference: EA 29795

To appear in: *Electrochimica Acta*

Received date: 30-1-2017
Revised date: 25-6-2017
Accepted date: 26-6-2017

Please cite this article as: Richa Pandey, Nan Jian, Alexandra Inberg, Richard E.Palmer, Yosi Shacham-Diamand, Copper Metallization of Gold Nanostructure Activated Polypyrrole by Electroless Deposition, Electrochimica Actahttp://dx.doi.org/10.1016/j.electacta.2017.06.157

Copper Metallization of Gold Nanostructure Activated Polypyrrole by Electroless Deposition

Richa Pandey[a*], Nan Jian[b], Alexandra Inberg[a], Richard. E. Palmer[b], Yosi Shacham-Diamand[a]

[a]Department of Physical Electronics, Faculty of Engineering, Tel-Aviv University, Ramat-Aviv 69978, Israel

[b]Nanoscale Physics Research Laboratory, School of Physics and Astronomy, University of Birmingham, Edgbaston, Birmingham, B15 2TT, UK

Abstract

We report on the study of novel polymeric electrodes made by the selective, electroless plating, of Copper (Cu) films on gold (Au) nanostructure-modified polypyrrole (Ppy). The main aim of the work is to define the effect of Au nanoparticle seed preparation method on its catalytic properties for Cu electroless deposition. The Au nanostructures were produced by two different techniques, namely, cluster beam deposition from a magnetron sputtering/gas condensation source (with precise size and composition control) and electrochemical deposition. To carry out the research, polypyrrole films were first synthesized by electro-polymerization on Au (200 nm)/SiO_2/Si substrates, followed by modification of the polymer surface by either electroplating of Au nanoparticles or Au_{923} clusters deposition from a magnetron cluster source. The gold nanoparticle modified electrodes were subjected to copper electroless deposition for different time intervals. The morphology, growth and nucleation kinetics of the resulting copper film were studied by environmental scanning electron microscopy-Energy dispersive X-ray spectroscopy (ESEM-EDS), atomic force microscopy (AFM) and X-ray fluorescence (XRF). Although both nanoparticle type showed similar incubation time, a faster catalytic response, once deposition had been initiated, was observed when the polypyrrole film was modified with Au_{923} clusters. The incubation time was independent of cluster size and type. This could be explained by a simple model assuming that the incubation time depends on similar parameters for both nanoparticle types, such as metal-metal (Au-Cu) binding energy, crystallographic misfit (Au- Cu) and lateral growth of the copper film. Further discussion is

presented in this paper in attempt to explain the different growth rate of Cu film catalysed by the Au_{923} clusters and electroplated Au nanoparticles.

Keywords: Electroless deposition; ; ; ; , Polypyrrole, Gold nanostructures, Electroplating, Cluster beam deposition.

1. Introduction

Current state of the art in high performance electronics is based on rigid, planar and single crystal inorganic materials, notably silicon wafers [1–3]. However, these materials are not optimal for integration with the soft and curvilinear characteristics of most shapes in nature, i.e. the body and organs of humans, other animals and plants [4]. This disparity in material properties hinders wearable sensors and actuators development for a wide range of applications such as bodily function monitoring, disease screening and diagnosis and sophisticated human-machine interface. An alternative to the rigid silicon based electronics is to build electronics on flexible organic materials like insulating, conducting and semiconducting polymers[5]. Polypyrrole (Ppy) is one such multifunctional polymer, where the conjugation of π-electrons confers conductivity. However, the conductivity of polypyrrole depends on the polymer doping by inorganic anions [6]. This increases the conductivity while reducing flexibility and increases brittleness. An alternative route to polypyrrole effective conductivity improvement is by its surface metallization with noble or transition metals [7].

In recent decades, the metallization of polymers has attracted a great deal of interest due to its potential application in sensors [8,9], conducting wires [9] and anti-electrostatic coating. The synergistic properties of hybrid structures based on a combination of conducting metals and flexible polymer enable a novel scheme for the development of polymeric MEMS, biosensors and implantable electrodes. Metallization of the polymers is usually done by physical vapour deposition (PVD), electroplating (on a seed layer) or electroless deposition [10]. Among these

various methods, electroless deposition has the advantage of being relatively simple with low processing temperature. It enables deposition on conductive and insulating surfaces, provides good via/trench filling and selective deposition. Electroless plating also requires relatively simple, low cost and scalable tools and infrastructure. However, electroless deposition of metal on polymer requires a surface catalytic layer (or in some cases a sub layer) to initiate the nucleation and growth of the plated metal film. Copper electroless deposition has been performed on polypyrrole using the traditional method of surface activation by $SnCl_2$ / $PdCl_2$ [11,12]. This method is widely used with good results, although it was pointed that in some cases the Sn and Pd may act as contaminants[13]. Another very practical method of seeding is the deposition of very thin noble metal film on the polymers of interest [14]. The catalytic layer can be in the form of continuous film or as nanoparticles. For nanoparticle seed, its catalytic efficiency depends on many variables such as the particle size, shape, morphology, distribution and purity as well as its deposition method. A seed layer of noble metal such as gold (Au) can be deposited on the polymer surface by several methods: chemical (colloidal route), electrochemical (electrodeposition) or physical (from the gas phase). The Au nanoparticles synthesized by chemical or electrochemical routes can suffer from limited purity and size control in the sub-nanometric size regime. Au nanoparticles produced in the gas phase are commonly called clusters when they contain less than about 10^4 atoms, corresponding to a size of a few nanometres. They are generally rather pure and ligand-free (naked) compare to the particles produced by solution-based methods. Various properties like particle size, crystallinity, degree of agglomeration, porosity, chemical homogeneity, and stoichiometry can be controlled with relative ease in the case of gas phase cluster synthesis by either adjusting the process parameters or adding an extra processing step, e.g., sintering (post-deposition) or size selection (in the gas phase) [15–18].

Models of electroless deposition at the nanoscale can be derived from conventional models of electrochemical deposition, although there is a fundamental difference: the total current in electroless deposition is zero. The mechanism of thin-film electroless deposition has been intensively discussed in the literature [19-22]. It is assumed to be characterized by three processes: nucleation (nuclei formation), growth, and coalescence of three dimensional crystallites (TDCs) [22]. In our case, we provide the necessary nucleation sites using catalytic metal nanoparticles. However, we cannot ignore the details of the nucleation stage since, as we will show later, the critical radius of nucleation is much smaller than the nano particle itself. A classical treatment of the nucleation during electroplating appears in the paper by Hills *et al* [23]. A key issue in the model discussed there is that the activation energy for electro-crystallization in the process of electroless deposition is related to the maximum of the excess free energy of the nucleus, which is determined by the critical radius. In this case the maximum free energy is determined by taking decreasing free energy into consideration. This excess free energy depends on the nano crystal volume and its increasing surface dimensions.

A transient model of electroless deposition appears in the paper by Ramasubramanian *et al* [24], where the fundamental equations are presented and solved numerically for the case of a flat surface. However, it is good to consider that this model is ideal for hemispherical features. The deposition on 3D nanoscale features (nanoparticles) requires special attention, as initial 3D effects may influence the diffusion between nuclei. For treatments of nanoscale deposition that underpin the work presented here, the reader is referred to the recent review paper by Zangari [25]: although it does not refer specifically to electroless deposition, it addresses key phenomena.

In this paper we report on a study of the catalytic properties of the Au nano-catalysts on the nucleation and growth of Cu films deposited by electroless deposition (ELD) on a nanoparticle-modified surface of an electro-polymerised polypyrrole film. The nanoparticle catalysts

employed were either size-selected Au_{923}(M) clusters produced by cluster beam deposition from the gas phase or electroplated gold nanoparticles AuNP(E), and the results were compared. The morphology of the Cu film was investigated by Environmental Scanning Electron Microscopy-Energy Dispersive X-ray spectroscopy (ESEM-EDS), High Angle Annular Dark Field (HAADF) Scanning Transmission Electron Microscope (STEM) and Atomic Force Microscope (AFM). The thickness of the Cu films was measured by X-ray Fluorimeter (XRF). The experimental data is complemented by a qualitative theoretical model of electroless deposition on nano-scale features, obtained by extending existing models of electroless deposition.

2. Experimental

2.1 Materials and Methods

All chemicals of the ACS grade were purchased from Aldrich Chemicals. The electrochemical polymerization of polypyrrole was carried out on Au (200 nm)/Ti (10 nm)/SiO_2/Si substrates in bath contained pyrrole (C_4H_5N) and lithium perchlorate ($LiClO_4$) in acetonitrile (CH_3CN). A Pt plate was used as a counter electrode and Calomel (KCl saturated) (SCE) was employed as a reference electrode. Pre-selected potential range was scanned between 0.0 and 1.2 V vs. SCE. Ppy films were deposited for 40 cycles with a scan rate of 50 mV/s.

Gold nanoparticles were electrodeposited on the polypyrrole from an electrolyte containing potassium dicyanoaurate ($KAu(CN)_2$), citric acid monohydrate ($C_6H_8O_7xH_2O$), and potassium hydroxide (KOH) to adjust pH = 4.5, at an operating temperature of 50˚C. Platinum plate was used as anode and the solution was stirred continuously. A fixed current density of J= 4 mA/cm^2 for 10 min was applied at the regime that allows the most controlled particles growth with good particle distribution[26].

The size selected Au_{923} clusters were generated by a magnetron sputtering, gas condensation cluster source equipped with a lateral time-of-flight mass selector[18,27]. The flow rates of Ar and He gas were 200 sccm and 150 sccm respectively. The condensation length used in this experiment was 250 mm. The cluster density can be controlled by the cluster beam current and the deposition time. The desired cluster density is 3 clusters/100 nm^2. The deposition energy of cluster was 0.5 eV/atom.

The composition of Cu ELD solution is presented in Table 1. Au nanostructure modified Ppy electrodes were dipped in the Cu ELD bath maintained at a temperature of 72˚C for different times. The AuNP(E)/Ppy was coated by Cu for 90, 120, 300 ,420 and 540 s whereas, Au_{923} (M)/ Ppy was coated for 50, 90,120, 420 and 540 s. After ELD the samples were washed thoroughly in DI water, and then dried with N_2 flow.

2.2 Characterization

The AuNP(E) electroplated on Ppy as well as the nucleation and Cu film growth were studied by Quanta 200 FEG Environmental Scanning Electron Microscope (ESEM). Whereas, Au_{923}(M) cluster were deposited on Cu grids coated by Ppy and were imaged by a JEOL JEM2100F STEM with a CEOS Cs-corrector[28]. The particle size and particle number in both the cases was evaluated by the image processing with ImageJ (NIH) software[26].

The Cu content (Wt%) in the samples was detected by Energy dispersive X-ray spectroscopy. Surface morphology and roughness were investigated by Atomic force microscopy (AFM MI150) in tapping mode for 20x20µm. X-ray reflection fluorimeter (Fischerscope® X-Ray XAN®-FD) was used to measure the Cu film thickness. The XRF was calibrated for “Cu films on plastic substrate” module was used for all the measurements.

3. Results and Discussion

ESEM image of electroplated AuNP(E) on polypyrrole is presented in Fig.1a. Sparsely distributed AuNP(E) can be seen all over the Ppy. The inset in Fig. 1a shows that the particles

have a wide size distribution. The average size of the nanoparticles was found to be 50±5 nm (inset Fig.1.a). A HAADF-STEM image of the Au_{923}(M) clusters is shown in Fig.1b. In contrast to AuNP(E), the clusters of uniform size of 6±0.5 nm (inset Fig.1b) are uniformly distributed on the Ppy surface. The calculated number of particle was found to be 2200/cm^2 and 3x 10^{12} /cm^2 for AuNP(E) and Au_{923}(M), respectively. This huge difference in the surface area contributes in the improved catalysis of Cu film formation by Au_{923}(M) as shown later in this work.

The morphology of the Ppy surface after Cu ELD is presented in Fig. 2.1. Formation of Cu/Au NPs on the electroplated AuNP(E) surface after 120 s of Cu electroless deposition was observed (Fig. 2.1a.). While after 300 s of ELD the Cu islands appears due to coalescence of the various nearby Cu/Au NPs (Fig. 2.1b). Further, Cu film growth (420 s) allows formation of Cu film with very globular morphology (Fig. 2.1c). For Ppy activated by Au_{923}(M) cluster, continuous Cu layer was observed on the surface after very short time of ELD (Fig. 2.1d). It indicates formation of smooth thin film right after 120 s of deposition (Figs. 2.1e,f). In both cases a gradual increase followed by saturation of the Cu content on the substrate is observed with the increase in deposition time (Fig. 2.2). The incubation time can be roughly estimated to be less than 90s; however, more comprehensive study of incubation time is performed by XRF later in the paper.

The dependence of Cu film surface roughness (RMS) on the time of its deposition is shown in Fig. 3. Two different trends were observed in the RMS vs time graph. In the case of the AuNP(E), there is a sudden increase in the roughness in 50 s then a gradual decrease in the roughness w.r.t. time. Similar increase is seen in Au_{923} (M) at 50 s, however, it's less compared to the former case. This could be since the AuNPs(E) are almost ten times bigger than the Au_{923}NP(M) and hence it gives rise to a very uneven and rough surface. With the course of

time the roughness decreases slowly and reaches a constant value around 500 s for both cases (Fig. 3a). The roughness increases with the time (t)

$$t_i < t < t_f \quad (1)$$

Where, t_i and t_f are initial and final time of deposition (Fig. 3b). At t_f , the roughness reduces rapidly giving a smooth and shiny Cu coverage.

Fig. 4 depicts the relationship of Cu film thickness measured at different time of deposition obtained by XRF. The linear dependence of the Cu film thickness on the deposition time was observed for AuNP (E)/Ppy substrate when compared to Au_{923} (M)/Ppy. The calculated deposition rate of Cu on AuNP (E)/Ppy was found to be 20 nm/min (calculated from the slope of the best fitted linear region of the thickness vs time graph), which is slower than that on Au_{923} (M)/Ppy (85 nm/min). This demonstrates that Au_{923} (M) is the better catalyst for the Cu film growth than AuNP (E). Such effect may be explained by high purity, high surface density, high size uniformity and homogeneous distribution of Au_{923} (M) clusters on the Ppy compared to AuNP (E) one. The growth trend also seems to be very gentle in case of AuNP (E)/Ppy when compared to steep growth in Au_{923}(M)/Ppy.

In both cases, the deposition is initiated on the surface of the nanoscale catalytic metal. Note, that the incubation time is similar in both cases. Incubation can be due to various reasons, one of them is due to the nucleation time where classical models assume that it depends on the binding energy between the catalytic surface (gold in our cases) and the deposited metal (Cu for both) (Fig. 5). The film continues to grow laterally between the nanoparticles until almost full coverage is achieved. Once the surface is fully covered the thin film continues to grow vertically. For nanoparticle seeding the initial stage includes two parts (Fig. 5):

1. Nucleation of copper on the catalytic metal nanoparticles until reaching full coverage on the nanoparticle.
2. Lateral growth between the nanoparticles until coalescence.

Conventional models of nucleation in electroless deposition assumes an effective energy barrier E*, that depends on the reduction in the free energy during crystallization and the increase in the surface energy. This model is only an approximation since in our case the substrate is non-flat and the dimension of the critical nucleus is not much smaller than the catalytic nanoparticles size. The critical nucleus assuming an ideal spherical symmetry is given by [14]:

$$r^* = \frac{2\gamma\upsilon}{[nF(E_{me}-E_{red})]} \quad (2)$$

Where, γ is the surface tension, υ is the molar volume of the metal deposit, n is the number of electrons involved in the redox reaction, F is the Faraday constant, and (E_{me} - E_{red}) is the potential between the metal (Cu) deposited and the reducing agent. Calculating this critical value for the basic electroless deposition solution (Table 1) yields a value of about 0.3 nm [14]. Therefore, we can assume that the critical radius of nucleation is significantly smaller than the nanoparticles used in this work as nucleation centers and that the initial nucleation step occurs on the gold nanoparticles until coalescence is partial or complete. This is followed by lateral and vertical growth of copper islands. This happens until the gap between the initial nanoparticles is completely filled with electroless deposition, the lateral deposition stops and the growth becomes only in the vertical dimension.

Once nucleation occurs the deposition rate for basic electroless Cu deposition is assumed to be a function of four parameters: (a) the copper complex concentration, $C_{Cu\text{-}complex}$, (b) the reducing agent (Formaldehyde in our case) concentration C_{HCOH}, (c) the hydroxyl ion concentration OH^- and (d) the complexing agent (Ligand) concentration (e.g. EDTA):

$$R = K \cdot C^a_{\mathrm{Cu-complex}} \cdot C^b_{HCOH} \cdot C^c_{OH^-} \cdot C^d_{EDTA^{4-}} \quad (3)$$

The various constants a, b, c, d, are presented for the steady state in the literature for few cases [14]. There is no data regarding the dependence of the deposition rate during the transient on

the various concentrations at the electrode interface. In the text presented here we will assume that the main dependence of the deposition rate is on the concentration of the copper metal ions. This is an approximation that needs to be re-examined in the future. Next, we will take into consideration of the formaldehyde concentration. The treatment here is qualitative and a full numerical analysis of the system may shed more light on the actual kinetics of the initial stage of the surface coverage. The solution to the diffusion equation assuming a diffusion coefficient D_{Cu} of the Cu ions and surface reaction constant k_s can be estimated from the deposition rate at period past the initial incubation period where the deposition rate is constant. This is typically at times longer than 2 minutes. At much longer time the deposition rate starts to drop, typically after 20-25 minutes in conventional open bath at the 70-75˚C range, without agitation. The reaction constant can be estimated using the relation between the deposition rate and the flux of Cu ions towards the surface:

$$Flux = \frac{R \cdot \rho \cdot N_A}{M_W} \tag{4}$$

Where, ρ is the metal density [g/cm^3], M_W is the molecular weights [g/mole] and N_A is the Avogadro number. Assuming that the deposition rate depends only on the metal ion (Cu) concentration:

$$R\left[\frac{cm}{sec}\right] = R' \cdot [Cu]\left[\frac{mole}{L}\right] = R' \cdot 10^3 [Cu]\left[\frac{mole}{cc}\right]$$
$$= \frac{R' \cdot 10^3 [Cu]}{N_A} \cdot [Cu]\left[\frac{\#\ molecules}{cc}\ or\ cm^{-3}\right] \tag{5}$$

This can be written as:

$$Flux = \frac{R' \cdot 10^3 \cdot \rho}{M_W} \cdot [Cu] = k_s \cdot [Cu] \text{ or } k_s = \frac{R' \cdot 10^3 \cdot \rho}{M_W} \tag{6}$$

Where, R’ is the deposition rate divided by the Cu concertation near the electrode. The constant k_s has units of velocity [cm/s] and can be referred to as the surface reaction velocity.

Assuming a deposition rate of 14.16×10^{-8}cm/s for the Au_{923}(M) and 3.36×10^{-8}cm/s for the AuNPs(E) (Fig.4, given M_W=63.546 g/mole and density of 8.92 g/cm^3 of Cu , the effective surface reaction velocity is 18.5×10^{-5} cm/s for the AuNPs(E) and 79.9×10^{-5} cm/s for the Au_{923}(M). A higher surface area in the case of Au_{923}(M) corresponds to higher surface reaction velocity as well as deposition rate when compared to AuNPs(E).

Solving the electroless deposition in one dimension, assuming the deposition rate depends only on the Cu concentration is given by[22]:

$$J = q \cdot n \cdot k_s \cdot c(x,0) \cdot \exp\left(\frac{k_s^2 \cdot t}{D}\right) \cdot erfc\left(\frac{k_s \cdot \sqrt{t}}{\sqrt{D}}\right) \quad (7)$$

Where D is diffusion coefficient of Cu ion, n is the number of electrons involved in the Cu ion reduction (n=2), c(x,0)=C_{Cu} (0) is the initial Cu concentration in the bath and k_s is the surface reaction velocity of the equation C_{Cu} --> C_{Cu2+}. We can define a critical time:

$$t_c = \frac{D}{k_s^2} \quad (8)$$

At very short time, t << t_c , the expressions is time independent:

$$J = q \cdot n \cdot k_s \cdot c(x,0) \quad (9)$$

While for long time, t >> t_c, we get

$$J = \frac{q \cdot n \cdot k_s \cdot c(x,0)}{\sqrt{\pi D t}} \quad (10)$$

This model can be extended for non-flat surface, specifically for hemi- spherical nuclei. Applying it to 2D and 3D yields a solution where the current at long time is not zero but reaches a value that actually depends on the radius of the spherical nuclei acting as an electrode. This yields an initial high deposition rate for the smaller particle in comparison to the larger nano particles. Therefore, we may assume that once Cu nano particle has been formed on the Au nanoparticle the nuclei on the smaller nano particles grow rapidly so the overall lateral growth is similar for both small and larger nanoparticles. Assuming D= 7×10^{-6} cm^2 /s for the Cu ion in the solution (in the complex form), the critical time for moving from surface reaction limited

regime to diffusion limited regime is in the range of several minutes to hours, thus we can conclude that at the initial deposition, the nucleation and growth is mostly surface reaction limited. Note that the numerical solution presented in [23] indicates that the surface reaction drops instantly at the initial stage of deposition but consecutively drops at a slow rate yielding almost constant deposition rate up to t >1000 s of deposition.

As stated before, the incubation time is very similar in both cases. Jacobs et.al [29] reported that small size particles retards the deposition due to nonlinear diffusion effect of dissolved oxygen towards smaller feature. The incubation time is also a function of binding energy of the substrate and the deposited metal and the crystallographic misfit between them[30]. The Au and Cu have same crystal structure (fcc) and the value of the lattice constant is more or less similar in both Au_{923}(M) clusters and AuNP(E). The binding energy of Cu-Au is also very similar in both the case. However, it could also be possible that the initial growth of the Cu on Au_{923}(M) is very fast which balances the slow growth of the Cu on AuNPs(E) until they coalescence and a film is formed.

4. Conclusion

A novel method of polypyrrole film metallization was studied. The Ppy surface was activated by two different Au nanostructures, electrodeposited AuNPs and Au_{923} clusters, before Cu electroless deposition. It was shown that the Cu film deposition rate depended on the substrate activation procedure. The copper deposition rate on the Au_{923}(M)/Ppy surface was at least three times higher than that on AuNP(E)/Ppy. It was understood in terms of the surface reaction velocity, which was found higher for small size and higher surface area, Au_{923}(M)/PPy sample. This behavior was explained by the small size of Au_{923}(M) catalyst features and their uniform distribution on the substrate. The copper film roughness as a function of its thickness was studied. Smoothening of the film with an increase in the Cu film thickness was observed. Two different trends in the roughness transformation during film growth demonstrate the extent of

influence of the catalytic surface texture and its nanostructure size on Cu ELD film. There are two possible mechanisms for the nucleation behavior that is observed and explained qualitatively in this work:

a. Effect of free energy of formation of the Cu deposition on the Au nanoparticles on incubation time.
b. The lateral growth of Cu between the nanoparticles after nucleation and growth of Cu on the Au nano particles themselves.

Once nucleation is reached, the deposition rate is rather constant. It should be noted that very similar incubation times for copper electroless deposition on both the Au_{923}(M)/Ppy and AuNP(E)/Ppy surfaces were observed. It was shown that the incubation time is not dependent on the size of the catalyst Au, but on various other factors like catalytic surface- deposited metal binding energy (Cu-Au), and their lattice parameters. Moreover, the incubation is also determined by the nature of the bath. This study provides groundwork on the effect of Au activation seed parameters on the Cu electroless deposition on polypyrrole.

Acknowledgments

The research leading to these results has received funding from the European Union's Seventh Framework Programme (FP7/2007-2013) under grant agreement no. 607417 (CATSENSE). The cluster beam deposition and STEM work were also supported by the Birmingham Science City project and EPSRC. We are grateful to Mr. Omri Heifler from Tel Aviv University Nanocentre and Oleg Kovalenko from Technion-Israel Institute of Technology for their efforts in acquiring the AFM results and to Ms. Stav Friedberg and Mr. Avi Yaverboim for the XRF measurements.

References

[1] G.E. Moore, Cramming more components onto integrated circuits (Reprinted from Electronics, pg 114-117, April 19, 1965), Proc. Ieee. 86 (1998) 82–85. doi:10.1109/N-SSC.2006.4785860.

[2] R.G. Arns, The other transistor: early history of the metal-oxide semiconductor field-effect transistor, Eng. Sci. Educ. J. 7 (1998) 233–240. doi:10.1049/esej:19980509.

[3] E. Vogel, Technology and metrology of new electronic materials and devices., Nat. Nanotechnol. 2 (2007) 25–32. doi:10.1038/nnano.2006.142.

[4] D.-H. Kim, R. Ghaffari, N. Lu, J. A Rogers, Flexible and stretchable electronics for biointegrated devices., Annu. Rev. Biomed. Eng. 14 (2012) 113–28. doi:10.1146/annurev-bioeng-071811-150018.

[5] M. Gerard, A. Chaubey, B.D. Malhotra, Application of conducting polymers to biosensors, Biosens. Bioelectron. 17 (2002) 345–359. doi:10.1016/S0956-5663(01)00312-8.

[6] A.G. MacDiarmid, Polyaniline and polypyrrole: Where are we headed?, Synth. Met. 84 (1997) 27–34. doi:10.1016/S0379-6779(97)80658-3.

[7] I. Dodouche, F. Epron, Promoting effect of electroactive polymer supports on the catalytic performances of palladium-based catalysts for nitrite reduction in water, Appl. Catal. B Environ. 76 (2007) 291–299. doi:10.1016/j.apcatb.2007.06.002.

[8] L. Torsi, M. Pezzuto, P. Siciliano, R. Rella, L. Sabbatini, L. Valli, P.. Zambonin, Conducting polymers doped with metallic inclusions: New materials for gas sensors, Sensors Actuators B Chem. 48 (1998) 362–367. doi:10.1016/S0925-4005(98)00058-6.

[9] V. Zaporojtchenko, T. Strunskus, K. Behnke, C. V. Bechtolsheim, A. Thran, F. Faupel, Formation of metal-polymer interfaces by metal evaporation: Influence of deposition parameters and defects, Microelectron. Eng. 50 (2000) 465–471. doi:10.1016/S0167-9317(99)00316-0.

[10] R.W. Burger, L.J. Gerenser, Metallized Plastics 3 : Fundamental and Applied Aspects, 1992. doi:10.1007/978-1-4615-3416-7.

[11] V.W.L. Lim, E.T. Kang, K.G. Neoh, Electroless plating of palladium and copper on polypyrrole films, Synth. Met. 123 (2001) 107–115. doi:10.1016/S0379-6779(00)00592-0.

[12] Y. Ohnishi, S. Yoshimoto, M. Kato, Metal pattern formation by selective electroless metallization on polypyrrole films patterned by photochemical degradation of iron(III) chloride as oxidizing agent, Synth. Met. 144 (2004) 265–269. doi:10.1016/j.synthmet.2004.04.015.

[13] S. Schaefers, L. Rast, A. Stanishevsky, Electroless silver plating on spin-coated silver nanoparticle seed layers, 2006. doi:10.1016/j.matlet.2005.05.085.

[14] Y. Shacham-Diamand, V. Dubin, M. Angyal, Electroless copper deposition for ULSI, Thin Solid Films. 262 (1995) 93–103. doi:10.1016/0040-6090(95)05836-2.

[15] F. Yin, Z.W. Wang, R.E. Palmer, Controlled formation of mass-selected Cu-Au core-shell cluster beams, J. Am. Chem. Soc. 133 (2011) 10325–10327. doi:10.1021/ja201218n.

[16] S.R. Plant, L. Cao, R.E. Palmer, Atomic structure control of size-selected gold nanoclusters during formation, J. Am. Chem. Soc. 136 (2014) 7559–7562. doi:10.1021/ja502769v.

[17] D.M. Wells, G. Rossi, R. Ferrando, R.E. Palmer, Metastability of the atomic structures of size-selected gold nanoparticles, Nanoscale. 7 (2015) 6498–6503. doi:10.1039/C4NR05811A.

[18] S. Pratontep, S.J. Carroll, C. Xirouchaki, M. Streun, R.E. Palmer, Size-selected cluster beam source based on radio frequency magnetron plasma sputtering and gas condensation, Rev. Sci. Instrum. 76 (2005). doi:10.1063/1.1869332.

[19] M. Paunovic and C. H. Ting, in Electroless Deposition of Metals and Alloys,M. Paunovic and I. Ohno, Eds., Proceedings, Vol. 12, Electrochemical Society, Pennington, NJ, 1988, p. 170. doi: 10.1007/978-1-4615-9576-2_30

[20] M. Paunovic and C. Stack, in Electrocrystallization, R. Weil and R, G. Barad as, Eds., Proceedings, Vol. 6, Electrochemical Society, Pennington, NJ, 1981, p. 205.

[21] R. Sard, The Nucleation, Growth, and Structure of Electroless Copper Deposits, J. Electrochem. Soc., 117, 864 (1970). doi: 10.1149/1.2407658.

[22] M. Paunovic, Electroless deposition of copper, in Modern Electroplating, Fifth Edition Edited by Mordechay Schlesinger and Milan Paunovic, pp. 433-446. John Wiley & Sons, Inc. (2010)

[23] G.Hills, A.K.Pour, B.Scharifker. The formation and properties of single nuclei. Electrochimica Acta, 28 (1983), 891-898. doi: 10.1016/0013-4686(83)85164-0

[24] M. Ramasubramanian, B. N.Popov, R. E.White, K. S.Chen, A mathematical model for electroless copper deposition on planar substrates. J. Electrochem. Soc., 146 (1999), 111-116. doi: 10.1149/1.1391572

[25] G. Zangari, Electrodeposition of Alloys and Compounds in the Era of Microelectronics and Energy Conversion Technology, Coatings 2015, 5, 195-218;

doi:10.3390/coatings5020195

[26] R.Pandey, R.O. Almog, Y. Sverdlov, Y. Shacham-Diamand, Self-Aligned Electrochemical Fabrication of Gold Nanoparticle Decorated Polypyrrole Electrode for Alkaline Phosphatase Enzyme Biosensing, J. Electrochem. Soc., 164, 4 (2017). doi: 10.1149/2.1401704jes.

[27] Z.W. Wang, R.E. Palmer, Determination of the ground-state atomic structures of size-selected Au nanoclusters by electron-beam-induced transformation, Phys. Rev. Lett. 108 (2012). doi:10.1103/PhysRevLett.108.245502.

[28] N. Jian, R.E. Palmer, Variation of the Core Atomic Structure of Thiolated (Au x Ag 1– x) 312±55 Nanoclusters with Composition from Aberration-Corrected HAADF STEM, J. Phys. Chem. C. 119 (2015) 11114–11119. doi:10.1021/jp5119103.

[29] J.W.M. Jacobs, J.M.G. Rikken, Oxygen-Diffusion-Size Effect in Electroless Metal Deposition, J. Electrochem. Soc. 135 (1988) 2822. doi:10.1149/1.2095440.

[30] S.H. Cha, H.-C. Koo, J.J. Kim, The Inhibition of Silver Agglomeration by Gold Activation in Silver Electroless Plating, J. Electrochem. Soc. 152 (2005) C388. doi:10.1149/1.190

Tables:

Table 1: Composition of electroless Cu deposition solution (Temperature=72˚C, pH=12.5)

Figures:

Figure.1. a) ESEM image of AuNP electroplated on Ppy, b) STEM image of Au_{923} clusters deposited by cluster beam source on Ppy; (Inset: size Vs count).

Figure.2. 2.1) ESEM image of Cu ELD on AuNP electroplated on Ppy for different time intervals a)120s, b) 300s, c)420s; ESEM images of Cu ELD on Au_{923} cluster deposited by cluster beam source on Ppy for different time intervals d) 50s, e) 90s, f) 120; (inset: EDX spectra) 2.2) The time of deposition Vs Weight% Cu graph obtained by EDX analysis (blue: AuNP (E)/Ppy; orange: Au_{923} (M) /PPy)

Figure.3. a) Time of Cu ELD Vs RMS roughness obtained from AFM (blue: AuNP (E)/Ppy; orange: Au_{923} (M) /PPy) b) Mechanism of Cu film formation elucidated from roughness analysis.

Figure.4. Thickness measurements Vs time graph obtained by XRF (green: AuNP (E)/Ppy; blue: Au_{923} (M) /PPy)

Figure.5. Initial nucleation (a) and growth (b) of electroless Cu on gold nanoparticle seed. Cu seed (light blue), Cu nuclei (dark blue) and Cu deposition (black) are represented. Arrows shows the diffusion of the ions from the bulk solution.

Figr-1**Figure 1:**

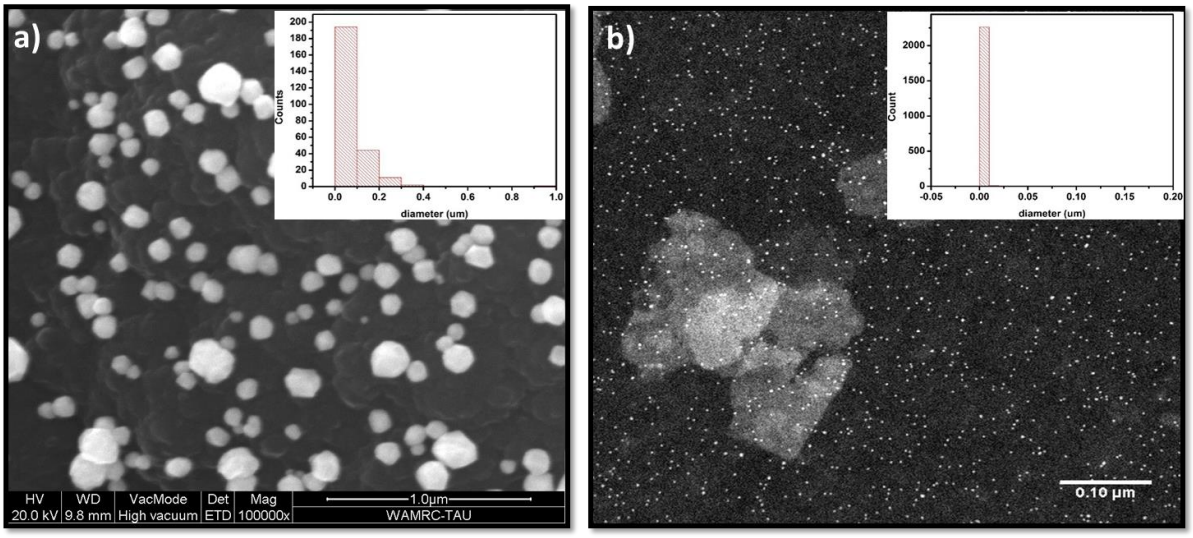

Figure 2:

2.1

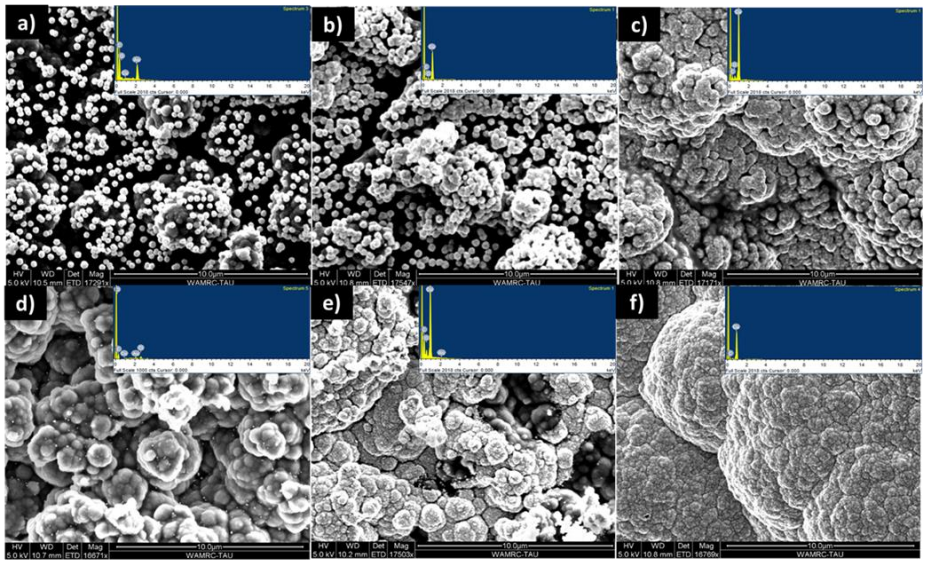

2.2

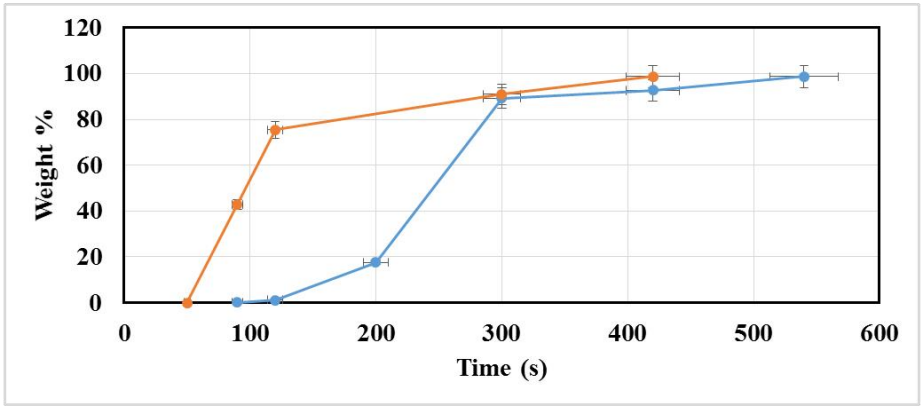

Figure 3:

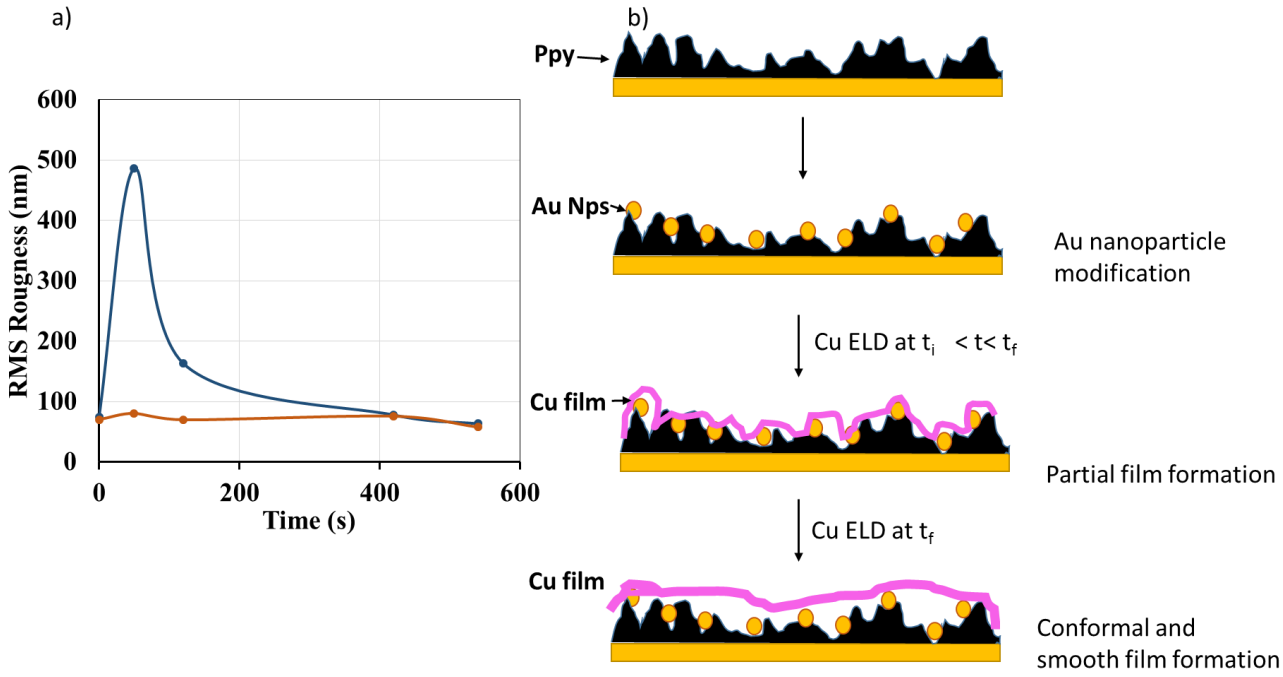

Figure 4:

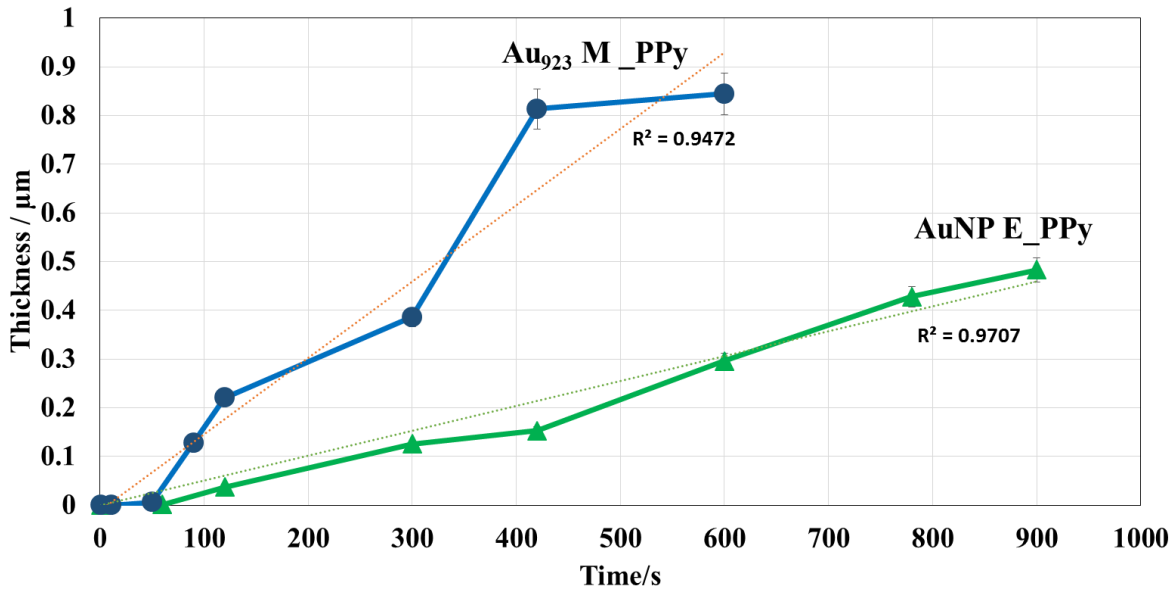

Figure 5:

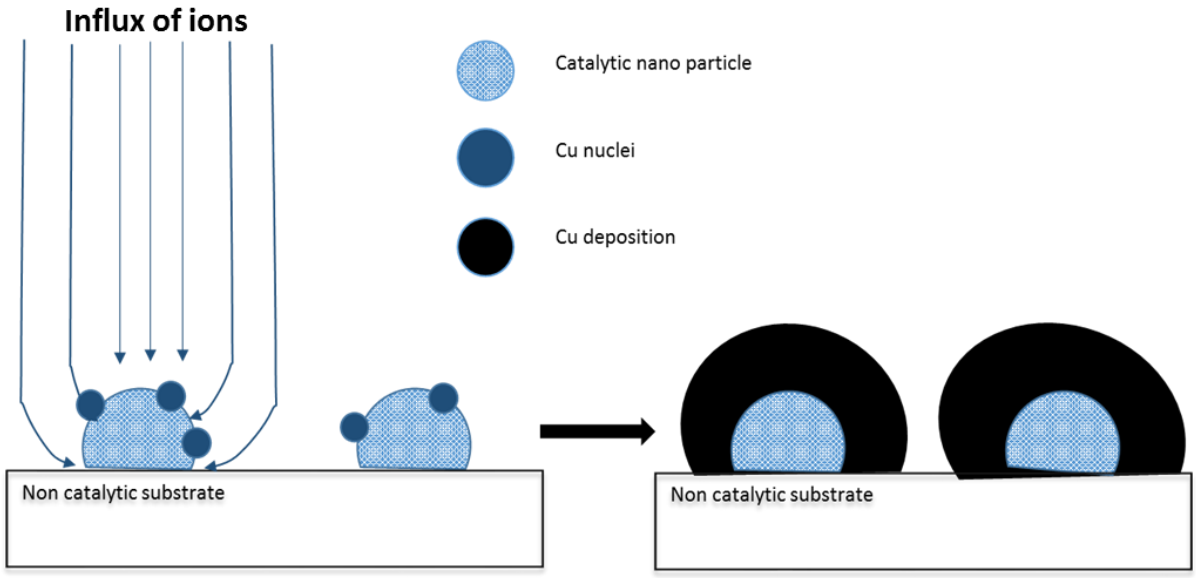

Table 1: Composition of electroless Cu deposition solution (Temperature=72˚C, pH=12.5)

	Amount [g/L]	Amount [M]
Copper sulphate pentahydrate, $CuSO_4.5H_2O$	7.6	0.03
Ethylene diamine tetra acetic acid, EDTA	14.6	0.049
Formaldehyde, HCOH (37%)	10	0.1
RE-610	0.05-0.1	~30 ppm
Potassium hydroxide, KOH	Adjust pH to 12.5	